STUDIA UBB CHEMIA, LXVI, 1, 2021 (p. 35-48)
(RECOMMENDED CITATION)
DOI:10.24193/subbchem.2021.1.03

POROUS SILICAS FROM MIXTURES OF $Na_2Si_3O_7$ AQUEOUS SOLUTION AND TEOS. INFLUENCE OF SODIUM SILICATE AMOUNT

ELENA-MIRELA PICIORUS[a], PAULA SVERA (IANASI)[b*], CATALIN IANASI[a*]

ABSTRACT. Silicon-based mesoporous materials have become increasingly used in various fields as industry, medicine, environment, etc. We developed five samples in mild conditions, at room temperature, of mesoporous silica by substituting tetra-ethyl-orthosilicate (TEOS) with different amount of sodium silicate ($Na_2Si_3O_7$) precursor by maintaining the total ratio for SiO_2 at 1.8g. Acetic acid (CH_3COOH)/hydrochloric acid (HCl) aqueous solution was used as catalyst keeping the pH at 5. The samples were examined by FT-IR, Raman Spectroscopy, Scanning Laser Confocal Microscopy and Nitrogen Adsorption-Desorption Isotherms. The results indicate enhancements when $Na_2Si_3O_7$ was added. Sample with TEOS and lowest amount of $Na_2Si_3O_7$ displayed the best surface area value (750 m^2/g) and total pore volume (0.63 cm^3/g). Highest amount of $Na_2Si_3O_7$ in the sample (P5) has considerably influenced the roughness of the material.

Keywords: *$Na_2Si_3O_7$, TEOS, mesoporous materials, roughness, porosity*

INTRODUCTION

Silica nanoparticles have received, in the last few years, an increased attention and interest of scientific community due to their wide applications such as photovoltaic cells [1], semiconductor electronic devices, catalysts and ceramics [2, 3]. In addition, amorphous SiO_2 nanoparticles are widely used for the fabrication of electronic substrates, thin film substrates, electrical and thermal insulators, humidity sensors and other applications. The silica particles

[a] *"Coriolan Drăgulescu" Institute of Chemistry, 24th Mihai Viteazul Bvd., 300223, Timişoara, România*
[b] *National Institute for Research and Development in Electrochemistry and Condensed Matter, 144th Dr.A.P. Podeanu Street, 300569, Timişoara, România*
**Corresponding authors, e-mails: cianasic@yahoo.com and paulasvera@gmail.com*

play an important role for each of these products. In some cases, the quality of these products is highly dependent on the size and size distribution of the silica particles [4-6]. The optical properties of silica nanoparticles can be attained with respect to the surface defects correlated with large surface/volume ratio. The synthesis of the SiO_2 nanoparticles can be achieved by several methods: combustion, plasma, hydrothermal and sol-gel processing [7-9]. Among these methods, the sol-gel method has an important advantage such as low temperature synthesis, control of reaction kinetics by varying the composition of chemicals, low cost and ease in controlling the properties of SiO_2, purity and homogeneity or other modifications of the material composition. In the past reports, the silica particles were synthesized from an expensive raw *material such as TEOS.* For many years, researchers have studied the sol-gel process starting from TEOS precursor. Bogush and Zukoski [10] obtained monodispersed silica particles with their sizes ranging from 40 nm to several micrometers using-controlled hydrolysis of tetraethylortho-silicate (TEOS) in ethanol, followed by condensation (polymerization) of the dispersed phase material. Simpler approach was conducted by Arenas et al. [11] that synthesized silica xerogels using only TEOS as precursor, acetic acid and acetone. They observed that the simultaneous addition of acetic acid, hydrochloric acids used as catalysts and acetone as solvent at room temperature (20 ^oC) conduct to the formation of amorphous silica materials with surface area up to 850 m^2/g and a pore volume of 0.24 cm^3/g. Dubey et al. [12] have synthesized silica nanoparticles for industrial applications using TEOS, ETOH, acetic acid and PVP as surfactant via sol-gel method. They obtained amorphous, mono-dispersed silica nanoparticles with 25 nm in diameter. Colloidal silica nanoparticles were synthesized by Lazareva et al. [13] starting from TEOS and by varying the catalyst type (HCl, NH_3), temperature of the thermal treatment (50-70 °C) and ratio of molar reactants, resulting in particles with sizes between 12 and 150 nm. Guo et al. [14] synthesized SiO_2 nanoparticles by sol-gel method using PEG 1000 as surfactant, TEOS as silica source and ammonia as catalyst. By varying the amount of PEG-1000 between 0.025 g and 0.1 g they obtained an average size of the particles between 9 and 35 nm.

However, using inexpensive source materials (Na_2SiO_3 or $Na_2Si_3O_7$) is required for the mass production of the SiO_2 particles. The molar ratio between silica and sodium oxide plays an important role in the chemical behavior of sodium silicate [15]. Chenge Liu [16] investigated the relationship between the rate of particle growth and factors as pH value, particle size, and the molar ratio of SiO_2:Na_2O. Many studies are using for their synthesized materials only sodium silicate as silica precursor without any other source of silica or template agent in order to obtain more ordered framework structures.

One example in this direction are synthesized silica nanoparticles via facile and economic sol-gel processing, using sodium silicate (Na_2SiO_3) as precursor [17]. They have obtained amorphous particles with almost well-defined and regular spherical structures, including a diameter of 25 nm. Ui et al. [18] synthesized mesoporous nanosilica powders from sodium silicate (Na_2SiO_3) in acid medium (pH 1-6), using anionic surfactant, sodium dodecyl sulfate (SDS). They demonstrated the pH influence over the surface area of the aforementioned synthesised materials, indicating a value of 1370 m^2/g in case of pH=3, which decreased to 984 m^2/g at pH=4. More studies regarding the pH influence were conducted by Hayrapetyan et al. [19], considering the effect of pH on the growth process of the colloidal silica sol particles.

However, few studies were made by substituting only the TEOS component with sodium silicate. Following this direction, Liu et al. [20] have synthesized mesoporous silica from mixtures of sodium silicate and TEOS in acetic acid/sodium acetate buffer (pH 4.4) using PEO-PPO-PEO as template. They obtained a surface area of 624 m^2/g for the sample where the content of sodium silicate was higher comparatively with the introduced amount of TEOS. Chun et al. [21] synthesized silica mesoporous from $Na_2Si_3O_7$ with TEOS and Pluronic F127 using supercritical method. Their observation regarding the synthesized TEOS based silicas under the supercritical CO_2 atmosphere include the increase of surface area by 3.8 times. Therefore, the formation of mesopores in $Na_2Si_3O_7$ and TEOS based silicas are resulted from collapsing micropores in supercritical CO_2 atmosphere. Fantini et al. [22] produced cage-like mesoporous silica using TEOS and sodium silicate in the presence of triblock copolymer template. Similar values for surface areas were obtained with both silica precursors. Mesoporous organosilicas [20] were prepared by using different silica precursor (organotrialkoxysilane with methyl, vinyl, 3-mercaptopropyl functionalities) and sodium silicate. The results show that the materials prepared from sodium silicate- organotrialkoxysilane have more ordered framework structure and narrower pore diameter distribution compared with the materials prepared from TEOS-organotrialkoxysilane. The organic-inorganic hybrid materials have higher surface area (between 890-1040 m^2/g) and pore volume (between 0.7-1.09 cm^3/g).

Herein, in our work, we used sol-gel route for the synthesis of mesoporous silica from mixtures of $Na_2Si_3O_7$ aqueous solution and tetraethylorthosilicate, both used as silica precursors (source of SiO_2), in CH_3COOH/HCl aqueous solutions (pH 5) without using any template. We have gradually replaced the TEOS with sodium silicate aqueous solution, because the $Na_2Si_3O_7$ is an economic raw material, environmentally benign and thermally stable. We selected to use acetic acid due to its ease dissolution in a wide variety of precursors, enabling a multitude of multi-cation solutions [23].

RESULTS AND DISCUSSION(S)

Infrared characteristics of sodium silicate xerogels

In order to confirm the presence of development of SiO_2, the samples were characterized using FT-IR analysis. The spectra of the samples dried at temperature of 100 °C are shown in **Figure 1**.

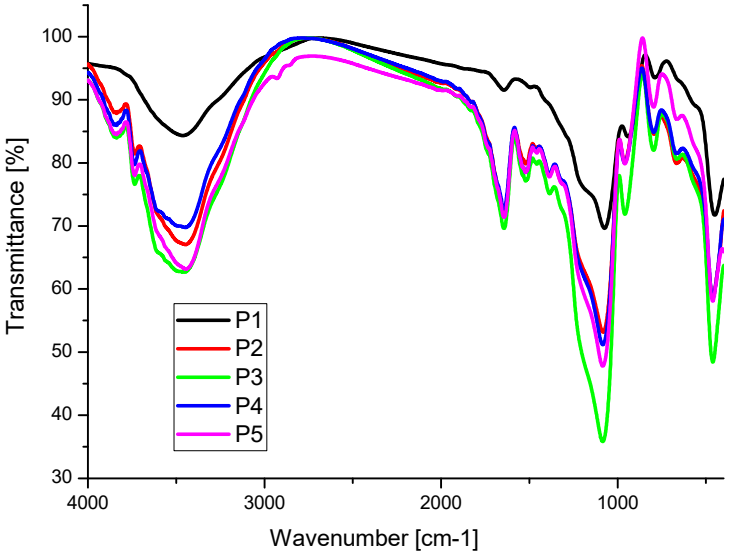

Figure 1. FT-IR spectra of the TEOS xerogels replaced with sodium silicate under acidic conditions

Silicate xerogels show the peaks of amorphous silica at 3463-3448 cm^{-1} and could be assigned to the stretching vibration of the H_2O molecules [24]. Same vibrations can be attributed to the -OH stretching on the silica surface which can also indicate the remaining water from the synthesis, indicating incomplete TEOS condensation [25]. The band appeared at 1646-1641 cm^{-1} is due to bending vibration of the H_2O molecules [26]. The broad band in the range of 1092-1060 cm^{-1} originates from the Si-O-Si asymmetric stretching vibration [27]. Absence of the 1168 and 812 cm^{-1} is an indicator for the low level of hydrolysis process [28] which may have been replaced by the condensation indicated in the literature [29]. The band at 959-942 cm^{-1} is due to the silanols groups and the Si-O stretching vibrations [30]. The changes in the intensity of the same band is an indicator for the level of the

hydrolysis and condensation level that occurs, whereas smaller peak indicates lower hydrolysis and therefore increased condensation [25]. It should be noted the fact that the Si-OH and Si-O- bonds have both specific bands closely located (960-920 cm^{-1}) which in present case is harder to evidence due to the band overlap [7]. The band at 794-781 cm^{-1} is responsible for the Si-O-Si symmetric stretching vibrations [31-34]. The bands at 474-455 cm^{-1} could be assigned to the Si-O asymmetric bending vibration of Si-O-Si [33]. In the literature the ≈960 cm^{-1} peak is also referred as an indicator for the C-H rocking vibrations specific for the methyl group present in TEOS [28]. Other carbon related groups interfering with the ones specific for the Si are presented by the O-C-C deformations located at ≈473 cm^{-1} [28]. In case of $Na_2Si_3O_7$ apart from the already aforementioned Si-O specific bonds, there are no expectations for other bands [35]. The pH during the synthesis influences greatly the results and therefore the peak intensities [35].

Raman Spectroscopy

In **Figure 2**(a), (b), the Raman spectra are shown for samples obtained by substituting tetra-ethyl-orthosilicate (TEOS) with different percent of sodium silicate ($Na_2Si_3O_7$) in two section of domain.

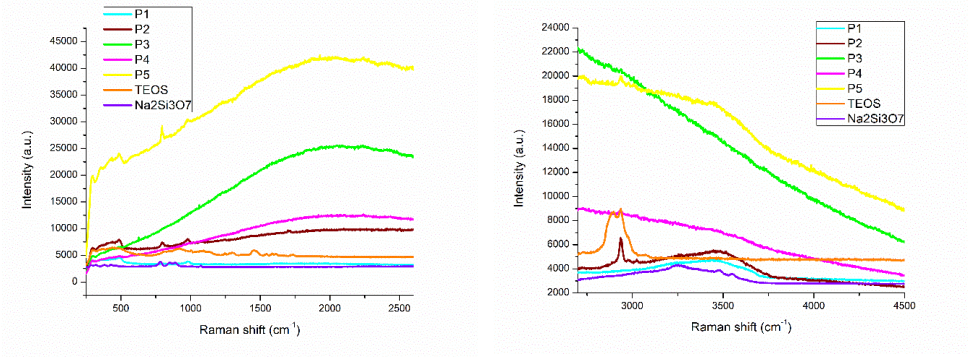

Figure 2(a), (b)**.** Raman spectra of the samples with different percent of sodium silicate ($Na_2Si_3O_7$)

For the TEOS sample, specific bands (200-400, 430-490, 500-651, 812-815, 865-890, 912-1008, 1048, 1096, 1110-1135, 1195-1292, 1454-1481, 1500-1700 cm^{-1}) were confirmed accordingly to the literature [36,37]. The most prominent bands are located at 438, 914, 1008, 1096 and 1135 cm^{-1}.

Si-O peaks which are expected for both TEOS and $Na_2Si_3O_7$ materials are generally observed in the 540-440 cm^{-1} region, with a specific broad band, accompanied by the presence of another specific peak around 950-1100 cm^{-1} [38,39]. In addition, siloxane rings which were also detected in the 1000-1300 cm^{-1} area, correspond to the asymmetrical Si-O stretching specific for dissolved silicates and solid glasses [36]. Other indicator for the amorphous glass type materials is the intensity of the 531-480 cm^{-1} Si-Si bond stretching, whereas the higher value indicates presence of metallic silicon compounds while lower value indicates the presence of amorphous silicon materials [40]. More Si bonds were detected, such as Si-O symmetric stretching vibrations in the 700-1000 cm^{-1} range [36], Si-O-Si stretching vibrations at 809 cm^{-1} [41] or 1049 cm^{-1} [37], symmetric stretching of Si-OH at 960 cm^{-1} [41] and asymmetric stretching of Si-O-C at 1906 cm^{-1} [41]. Wide band in the 430-490 cm^{-1} region is visible due to the silane bond bending [37]. Raman peaks in the region of 600-650 cm^{-1} are resulted from the connections between alkoxy groups and silicon atoms, which are also an indicator for the hydrolysis efficiency [37]. According to the literature the peak around 651 cm^{-1} is representative for the TEOS molecules consisting of four ($-OC_2H_5$) groups connected to the silicon atom [37]. This peak also is the main indicator for the hydrolysed TEOS [37], which is gradually replaced by the condensation reaction that takes place instead [29]. The hydrolysis-condensation processes are a consequence of the pH, solvent and H_2O amount used in the synthesis and as a result acid or base-catalysed displacement reactions that take place [29]. The displacement reactions are represented by the protonation of OH or OR substituents bounded to the Si (in acidic conditions) or by the direct attack of the hydroxyl or silanolate anions to the Si (in the basic conditions) [29]. In the material it is observed the presence of the silica-methyl group's connectivity indicated by the 460 cm^{-1} band [41] which may be overlapped by the 400-450 cm^{-1} SiO_2 stretching bonds [37]. In addition, rocking C-H (760 cm^{-1}) [41], C-H asymmetric bending (1412 cm^{-1}) [41], C-H symmetric stretching (2907 cm^{-1}) [41, 42] and C-H asymmetric stretching (2974 cm^{-1}) vibrations are also present [41]. According to other studies the 880 cm^{-1} is assigned to C-C-O stretching [37] as a consequence of low hydrolysis that takes place. Si-C bonds were also registered in the Raman spectra, being confirmed by the presence of the 1250 cm^{-1} peak [42]. The existence of silanols and silicon oxide bands on the surface is evidenced by the 977 cm^{-1}, respectively the 1096 cm^{-1} peak [42].

Regarding the $Na_2Si_3O_7$ sample, vibrational energies of Na-O were expected and found below 300 cm^{-1} area [36]. It should be mentioned that this Na-O bonds have less influence on the Si-O bonding, expecting less modifications in the 1000-1300 cm^{-1} area. In the same work [36] it is mentioned

that materials prepared in basic conditions, have achieved higher intensity values in comparison to the acid media prepared materials. Using alcohol in the synthesis may also affect the structure orientation of the silica materials [36]. The 780 cm^{-1} peak which is only present in case of $Na_2Si_3O_7$ also indicates the presence of Si monomers, whereas the 485 cm^{-1} peak is an indicator of siloxane rings [36]. Symmetric deformation (δ_s) at 423 cm^{-1} was assigned to the (X) O-Si-O(X) where x is presented as Na, H, or negative ionic charge [38, 43]. The higher intensity of 1050 cm^{-1} peak in comparison to the one located at 980 cm^{-1} is suggesting (in both TEOS and $Na_2Si_3O_7$) that the doubled siloxane rings are not suffering any breakage [36]. The two peaks located around 450 and 650 cm^{-1} are showing the siloxane rings, in this case, the TEOS having less since the 450 peak is lower in intensity [36]. Peaks below 300 cm^{-1} may show the breakage of large siloxane rings that contain more than 6 members.

When comparing the P1, P2, P3, P4, P5 and the precursors (TEOS and $Na_2Si_3O_7$), overall signal intensity is different, suggesting fluorescence interference. The higher energy excitation source (514 nm visible laser) can strongly influence the appearance of the spectra [44], still the main peaks for the Si based compounds are observed as expected around 971 cm^{-1}, together with ≈801 cm^{-1} and ≈501 cm^{-1} followed by the less prominent peaks under 501 cm^{-1}.

Scanning Laser Confocal Microscopy

A series of images were captured, at 10x and presented in **Figure 3**. The samples show tempered glass chips like appearance of the crystals, with various size and shapes. The obtained images show differences with the increasing Na content and decreasing TEOS content, revealing unlike presence of triangle and pyramidal shaped like crystals, which are visible in case of sample P4 and less in P5. With the maximum 2.5 g Na, the P5 crystals shrink to smaller dimensions.

Calculated roughness values from the 50x images (see **Figure 4**) (Average roughness (Sa), Mean Square Root Roughness (Sq), Maximum peak height (Sp), Maximum valley depth (Sv), Maximum peak-to valley height (Sz), Surface kurtosis (Sku), Surface skewness (Ssk)) for P1, P2, P3, P4 and P5 samples are shown below in **Table 1**.

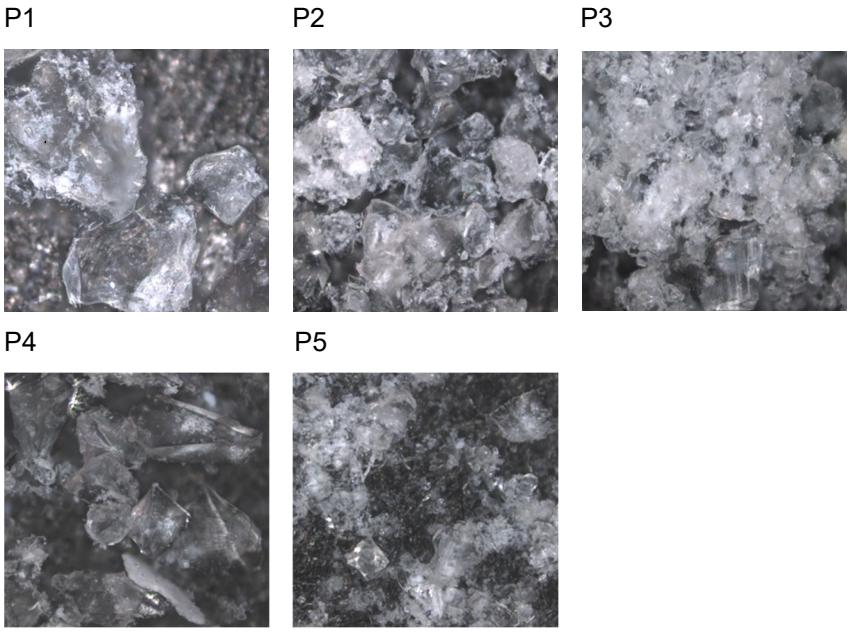

Figure 3. Images of samples obtained at 10x

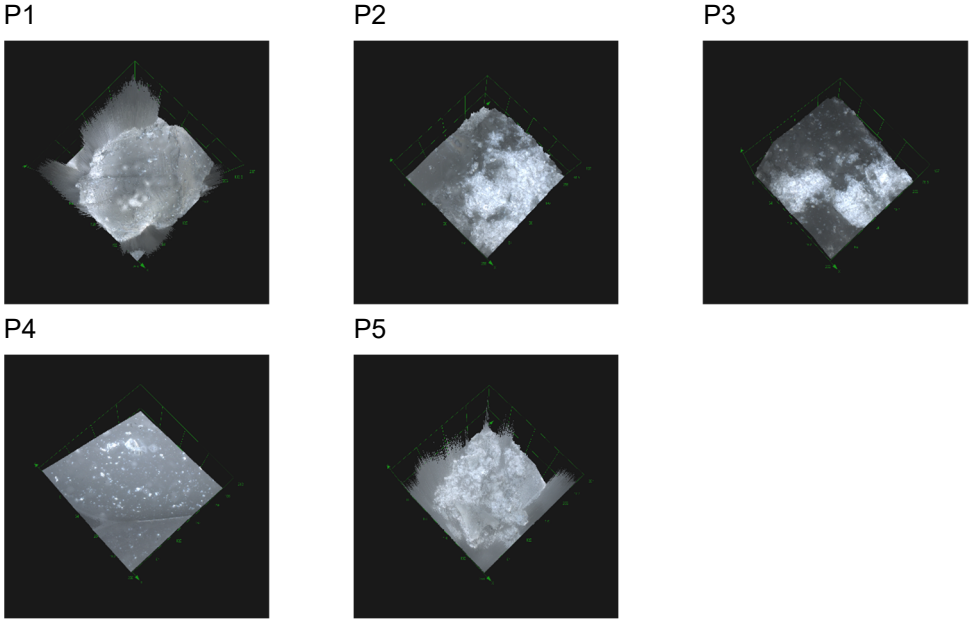

Figure 4. Images obtained for silica nanoparticles

Table 1. Data parameters for silica nanoparticles

Whole area (258 µm x 258 µm)	Average roughness (Sa)	Mean Square Root Roughness (Sq)	Maximum peak height (Sp)	Maximum valley depth (Sv)	Maximum peak-to valley height (Sz)	Surface kurtosis (Sku)	Surface skewness (Ssk)
P1	12.984	20.540	140.365	67.171	207.536	8.77	1.056
P2	4.046	5.570	93.368	50.002	143.370	5.100	-0.149
P3	2.988	4.416	76.284	69.074	145.358	7.174	-0.062
P4	1.506	5.270	154.246	31.426	185.672	4.133	-1.592
P5	9.202	13.276	79.037	29.641	108.677	7.145	-1.467

Roughness parameters are used for characterizing the roughness of a material, whereas the most important parameters are Sa and Sq. Both Sa and Sq parameters indicate the average roughness of the material using different calculation formula. For the analysed materials, highest average roughness is attributed to the P1, followed by the P5, P2, P4 and P3 sample. High rugosity in case of the P5 resulted due to the presence of very small crystals and therefore inability to analyse the surface of one single crystal as it was in the case of the rest of the samples.

Ssk (skewness) is sensitive to the peak/valley overall tendency on the surface of the material, whereas positive skewness (Ssk > 0) is more present in case when high spikes protrude above a flatter average distribution, and negative skewness (Ssk < 0), on the other hand, indicate deep valleys in a smoother area, which is more specific for porous materials. In our case only one sample has positive skewness, which is also visible from the 2d image of the sample (P1) presenting large crystals.

All samples show the presence of inordinately high peaks and low valleys based on the kurtosis (Sku) sharpness parameter of the profile (Sku > 3) which is probably due to the “tempered glass chips” nature of the sample, with occasional geometric morphologies that also imply the presence of more edges.

Textural Characteristics

The N_2 adsorption–desorption isotherms are given in **Figure 5**.

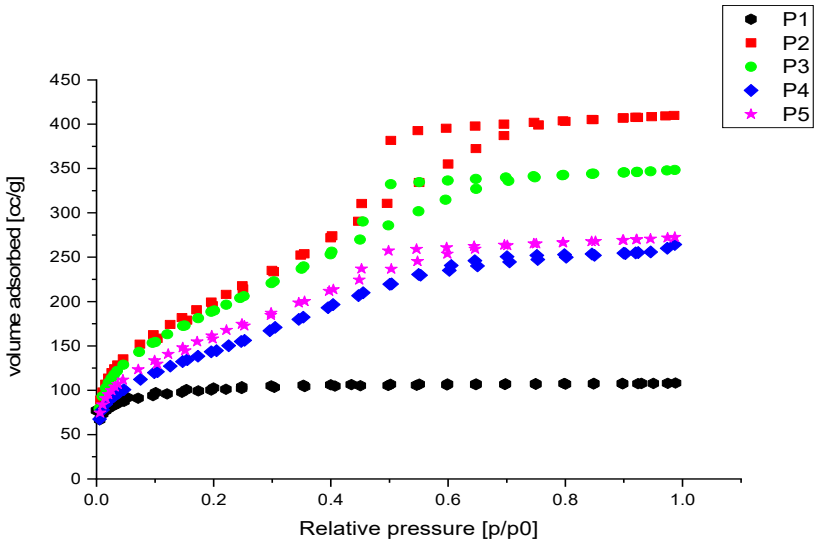

Figure 5. N_2 adsorption -desorption isotherms of silica nanoparticles

According to the International Union of Pure and Applied Chemistry (IUPAC) [45], N_2 adsorption-desorption isotherms of silicate xerogels produced are Type Ib in case of sample P1, Type IVa for samples P2, P3, P5 and Type IVb for sample P4. The type Ib isotherms are specific for materials with wider micropores and possibly narrow mesopores under 2.5 nm. In case of type IVa isotherms, the materials are characteristic for mesoporous materials and capillary condensation is accompanied by hysteresis [45, 46]. The hysteresis obtained for samples P2, P3 and P5 showed H2b type of hysteresis loops characteristic for complex pore with larger neck widths. In case of sample P4 the type IV b isotherm is specific for mesopores with smaller width. **Table 2** shows the parameters obtained from isotherms for the silicate xerogels prepared.

Table 2. Textural parameters and data obtained from isotherms

Sample name	DFT Pore width, [nm]	BJH Desorption Pore diameter [nm]	Multi-BET surface area [m^2/g]	Total pore volume [cm^3/g]
P1	2.50	3.068	316	0.17
P2	5.09	3.853	750	0.63
P3	4.89	3.450	702	0.54
P4	4.89	3.451	529	0.41
P5	3.40	3.443	591	0.43

Using DFT method, pore size distribution profiles of prepared silicate xerogels are given in **Figure 6**.

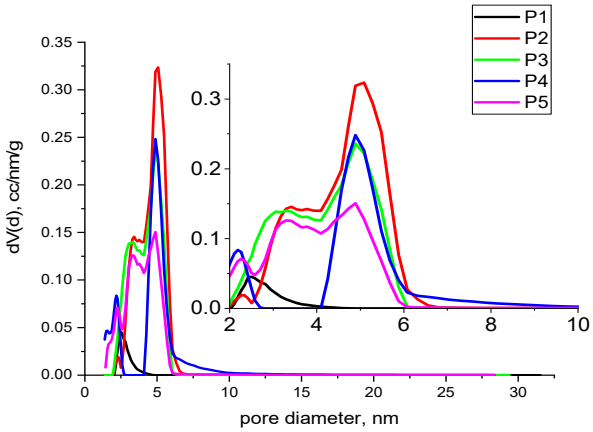

Figure 6. Pore size distribution of silica nanoparticles

From **Figure 6** we can observed that in case of sample P1 the material presents a large unimodal distribution with an average of 2.5 nm and for sample P4, the material presents a bimodal distribution with an average of 4.89 nm. In case of the all-other samples the distribution of pores is multimodal confirming the type of isotherms.

The sample P2 has the highest surface area and a total pore volume of 750 m^2/g and 0.63 cc/g respectively. Pore size distribution was affected by the gelation pH (high content of sodium silicate). The sample P2 presents also the largest pore size of 5.09 nm.

CONCLUSIONS

Silica xerogels with high surface area, highly uniform pore structure and high silanol group content were successfully synthesized using low-cost silica source ($Na_2Si_3O_7$) and TEOS in the presence of acetic acid and hydrochloric acid via sol–gel process. The use of acetic/HCl acid in sodium silicate sol-gel process was important because them produce high surface area of mesoporous materials without addition of any template agent.

The simultaneous addition of acetic/HCl acid as catalysts and used of acetone as solvent, made possible to synthesize amorphous silica nanomaterials with high surface area and pore volume. The highest BET surface area of 750 m^2/g and pore volume 0.63 cm^3/g was registered for P2

sample. Also, all xerogels silicate samples were kept at room temperature for gelling, the temperature being another parameter satisfactory to obtain the high surface area. FTIR spectra reveal the main characteristic bands for porous SiO_2 nanoparticles. Raman spectra certifies the structure of porous SiO_2 nanoparticles and emphasizes the presence of both hydrolysis and condensation processes which are also confirmed by the FTIR spectra. Laser confocal images put in evidence the influence of the TEOS/$Na_2Si_3O_7$ amount on the crystal size and rugosity.

EXPERIMENTAL SECTION

Materials

Tetra-ethyl-orthosilicate (TEOS, 98% Merck), acetone (CHIMREACTIV SRL, 99.92%), $Na_2Si_3O_7$ (Loba Feinchemie), acetic acid (Chimopar, reactive analysis), Hydrochloric acid (HCl, EMSURE ^{R}, ACS, ISO, Reag Ph. EUR 37%), distilled water without further purification.

Xerogels synthesis

A series of five sample of silica was prepared using different quantities of sodium silicate ($Na_2Si_3O_7$) by replacing TEOS and maintaining the total ratio for SiO_2 at 1.8g. We solubilized the $Na_2Si_3O_7$ in different amounts of distilled water in order to obtain a molar ratio of 1:722. Then, TEOS was solubilized in acetone and form a second solution and added drop wise onto the first solution. We added a 1: 9 solution of CH_3COOH/HCl in order to adjust the pH at 5. The precursors for the synthesis are shown **in Table 3**.

Table 3. Synthesis parameters

Samples	P1	P2	P3	P4	P5
TEOS (g)	6.5	3.3	1.9	0.6	0
$Na_2Si_3O_7$ (g)	0	1.25	1.75	2.25	2.5
Acetone (g)	10	10	10	10	10
CH_3COOH(g)	3	3	3	3	3
HCl (mL)	0.1	0.1	0.1	0.1	0.1
H_2O (g)	3	65	91	117	130

The solutions were left to gel and were stored for 28 days at room temperature for ageing. The obtained materials were washed in excess with water for 5 times and 2 times with ethanol. The obtained materials were dried at 100 ^oC and further analyzed.

Characterization

The chemical structure of sodium silicate xerogels was confirmed by using FT-IR spectrometry (JASCO 430 apparatus) in the wave number range of 4000 to 400 cm^{-1}. Raman spectra was done with Shamrock 500i Spectrograph from Andor United Kingdom.

Imaging and roughness data were obtained with LEXT – 3D measuring laser microscope OLS4000 with 405 nm laser light source.

Nitrogen adsorption measurements were carried out at 77 K with a Surface Area and Pore Size Distribution Analyzer (Quantachrome Nova 1200e) to determine the pore size, pore volume and specific surface area of the xerogels obtained. Specific surface area was calculated by the Brunauer-Emmett-Teller (BET) method. Total pore volume was estimated from the adsorbed N2 volume at ~1 relative pressure (P/Po) values. Barrett-Joyner-Halenda (BJH) method was used to estimate pore size and pore volume by using desorption branch of the isotherm.

ACKNOWLEDGMENTS

The authors thank to „Coriolan Dragulescu" Institute of Chemistry of Romanian Academy for the financial support: Program 4. Inorganic compounds and hybrids with relevance in nanostructured materials science, precursors for advanced materials.

REFERENCES

1. N.P. Rizky; A.B. Herny; M.H. Agus; Sekartedjo and D.R. Doty; *Proc. Eng.,* **2017**, *170,* 93
2. G.H. Bogush; M.A. Tracy and C.F. Zukosky; *J. Non-Cryst. Solids* **1988**, *104,* 95
3. M. Sadeghi; M. Dorodian and M. Rezaei; *J. of Adv. In Chem.*, **2013**, *6*, 917-922
4. G. Herbert; *J. Eur. Ceram. Soc.* **1994**, *14*, 205-214
5. A.-M. Putz; L. Almasy; A. Len; C. Ianasi, *Fuller. Nanotub. Car. N.*, **2019**, *27,* 323-332
6. A.-M. Putz; C. Savii; C. Ianasi; Z. Dudás; K.N. Székely; J. Plocek; P. Sfârloagă; L. Săcărescu; L. Almásy, *J. Porous Mater.,* **2015**, *22*, 321-331
7. D. Nagao; H. Osuzu; A. Yamada; E. Mine; Y. Kobayashi; M. Konno; *J. Colloid Interface Sci.* **2004**, *279*, 143-149
8. S. Vemury; S.E. Pratsinis; L. Kibbey; *J. Mater. Res.,* **1997**, *12*, 1031-1042
9. T. Tani; N. Watanabe; K. Takatori; *J. Nanoparticle Res.,* **2003,** *5*, 39-46
10. G.H. Bogush and C.F. IV Zukoski *J. Colloid Interface Sci*, **1991**, *142*, 19-34
11. L.T. Arenas; C.W. Simm; Y. Gushikem; S.L.P. Dias; C.C. Moro; T.M.H. Costa, E.V. Benvenutti; *J. Braz. Chem. Soc.*, **2007**, *18*, 886-890
12. R.S. Dubey; Y.B.R.D. Rajesh; M.A. More; *Mater. Today Proc.*, **2015**, *2*, 3575-3579
13. S. Lazareva; N. Shikina; L. Tatarova and Z. Ismagilov; *Eurasian Chem.-Technol. J.*, **2017**, *19*, 295-302
14. Q. Guo; D. Huang; X. Kou; W. Cao; L. Li; L. Ge; J. Li; *Ceram. Int.,* **2017**, *43*, 192-193
15. A.A. Hamouda and H.A.A. Amiri; *Energies* **2014**, *7* 568-590

16. H.C. Liu; J.X. Wang; Y. Mao; R.S. Chen; *Colloid Surf. A Physicochem. Eng. Asp*., **1993**, *74*, 7
17. M.F. Zawrah; A.A. EL-Kheshen; H.M. Abd-El-Aal, *J. Ovonic Resear.,* **2009**, *5,* 129-133
18. S.-W. Ui; I.-S. Choi; S.-C. Choi; *Int. Sch. Res.*, **2014**, Article ID 834629, 1-6
19. S.S. Hayrapetyan; H.G. Khachatryan; *Microporous Mesoporous Mater*., **2005**, *78*, 151-157
20. N. Yu; Y. Gong; D. Wu; Y. Sun; Q. Luo; W. Liu; F. Deng; *Microporous Mesoporous Mater.* **2004**, *72,* 25-32
21. B.S. Chun; P. Pendleton; A. Badalyan; S.-Y. Park; *Korean J. Chem. Eng.,* **2010**, *27*, 983-990
22. M.C.A. Fantini, C.F. Kanagussuko; G.J. M. Zilioti; T.S. Martins; *J. Alloys Compd*., **2011**, *509,* S357-S360
23. T.H. Chiang; S.-L. Liu; S.-Y. Lee; T.-E. Hsieh; *Thin Solid Films*, **2009**, *517,* 6069-6075
24. P. Innocenzi; P. Falcaro; D. Grosso; F. Babonneau; *J. Phys. Chem. B*, **2003**, *107,* 4711-4717
25. E.C. de O. Nassor; L.R. Ávila; P.F. dos S. Pereira; K.J. Ciuffi; P.S. Calefi, & E.J. Nassar; *Mater. Res.*, **2011**, *14*, 1–6
26. H. El Rassy; A.C. Pierre; *J. Non- Cryst. Solids,* **2005**, *351*, 1603-1610
27. S.R. Ryu; M. Tomozawa; *J. Non-Cryst. Solids*, **2006**, *352*, 3929-3935
28. F. Rubio; J. Rubio; J.L. Oteo, *Spectroscopy Lett*., **1998**, *31*, 199-219
29. C.J. Brinker; J. Non Cryst. Solids, **1988**, *100*, 31-50
30. S.S. Prakash; C.J. Brinker; A.J. Hurd; *J. Non Cryst. Solids*, **1995**, *190*, 264-275
31. S. Musić; N. Filipović-Vinceković and L. Sekovanić; *Braz. J. Chem. Eng*., **2011**, *28,* 89-94
32. X. Ying-Mei, Q. Ji; H. De-Min; W. Dong-Mei; C. Hui-Ying; G. Jun and Z. Qiu-Min; *Oil Shale,* **2010***, 27*, 37-46
33. D. Geetha; A. Ananthiand and P. S. Ramesh; *J. Pure Appl. Phys.,* **2016***, 4,* 20-26
34. V.H. Le; C.N.H. Thuc and H.H. Thuc; Nanoscale Res. Lett., **2013**, *8*, 58
35. W. Thongthai and C. Metta; *Songklanakarin J. Sci. Technol*., **2012**, *34*, 403-407
36. I. Halasz; A. Kierys; J. Goworek; H. Liu; R.E. Patterson; *J. Phys. Chem. C*, **2011**, *115*, 24788-24799
37. G. Marcin; J.-S. Małgorzata; K. Mikko; S. Janne; *Proceedings, XVII IMEKO World Congress*, 2003, June 22 – 27, Dubrovnik, Croatia
38. G. Socrates; Infrared and Raman Characteristic Group Frequencies Tables and Charts, *John Wiley & Sons*, **2001**
39. T. Jin; Z. Shanrong; W. Weifeng; D. Gordon; M. Xuanxue; *Mater. Sci. Eng. B*, **2004**, *106*, 295
40. O.V. Khavryuchenko; V.D. Khavryuchenko; J.O. Roszinski; A.I. Brusilovets; B. Friede; V.V. Lisnyak; *Thin Solid Films,* **2006**, *515,* 1280
41. A. Jitianu; G. Amatucci; L.C. Klein; *J. Mater. Res*., **2008**, *23,* 2084
42. H. Haryadi; *IPTEK,* **2007**, *18*, 74
43. I. Halasz, R. Li; M. Agarwal and N. Miller; *Stud. Surf. Sci. Catal.*, **2007**, *170A*, 800
44. D. Cebeci; A. Alam; P. Wang; R. Pinal; D. Ben-Amotz; *Eur. Pharm. Rev*., **2017**, *22*, 18-21
45. K.S. W. Sing; D.H. Everett; R.A.W. Haul; L. Moscou; R.A. Pierotti; J. Rouquerol; T. Siemieniewska; *Pure Appl. Chem.,* **1985**, *57,* 603
46. M. Thommes; K. Kaneko; A.V. Neimark; J.P. Olivier; F. Rodriguez-Reinoso; J. Rouquerol and K.S.W. Sing; *Pure Appl. Chem*., **2015**, *87,* 1051